A 335–407-GHz SiGe-Based Subharmonic Mixer Using a Fully Integrated LO Generation

Jonathan Bott, *Graduate Student Member, IEEE*, David Starke, *Graduate Student Member, IEEE*, Florian Vogelsang, *Graduate Student Member, IEEE*, Jan Schöpfel, *Member, IEEE*, Christian Bredendiek, *Member, IEEE*, Klaus Aufinger, *Member, IEEE*, and Nils Pohl, *Senior Member, IEEE*

***Abstract*— This letter introduces a silicon–germanium (SiGe)-based subharmonic mixer (SHM) optimized for THz radar applications, operating at a center frequency of 360 GHz with a 3-dB bandwidth of 72 GHz. This mixer is a key component in a fully integrated receiver, featuring a wideband 90-GHz voltage-controlled oscillator (VCO), a frequency doubler stage, and power amplifier (PA) stages. The mixer exhibits a conversion gain of −6.1 dB while maintaining an excellent input compression point of >4 dBm, accompanied by a simulated noise figure (NF) of 24.8 dB. Moreover, a current consumption of only 8.6 mA underlines the energy efficiency.**

***Index Terms*— B12HFC, BiCMOS, frequency doubler, frequency multiplier, frequency-modulated continuous wave (FMCW), Lange coupler, power amplifier (PA), radar, receiver, silicon–germanium (SiGe), subharmonic mixer (SHM), voltage-controlled oscillator (VCO), wideband.**

I. Introduction

RESEARCH on THz circuits is motivated by specific applications where the advantages of sub-mm wavelengths outweigh the considerable challenges associated with circuit design [1], [2], [3], [4], [5]. Key applications benefiting from THz frequencies include radar and communication systems, where the large available bandwidth can improve target differentiation and enhance channel capacity, respectively.

Manuscript received 22 March 2024; accepted 9 April 2024. Date of publication 24 April 2024; date of current version 7 June 2024. This work was supported in part by German Research Foundation ("Deutsche Forschungsgemeinschaft") (DFG) under Project 287022738 TRR 196 for Project C02 and C03, in part by German Ministry for Economic Affairs and Climate Action [Bundesministerium für Wirtschaft und Klimaschutz (BMWK)] in the Project URBANSens within the Research Program LuFo VI-2 under Grant 20D2106B, in part by German Federal Ministry of Education and Research [Bundesministerium für Bildung und Forschung (BMBF)] in the Course of the 6GEM Research Hub under Grant 16KISK037, and in part by the Ministry of Culture and Science of the Federal State of North-Rhine-Westphalia in the Frame of "Netzwerke 2021" as part of the Project "terahertz.NRW" under Project NW21-068D. *(Corresponding author: Jonathan Bott.)*

Jonathan Bott, David Starke, Florian Vogelsang, and Jan Schöpfel are with the Institute of Integrated Systems, Ruhr University Bochum, 44801 Bochum, Germany (e-mail: jonathan.bott@rub.de).

Christian Bredendiek is with the Fraunhofer Institute for High Frequency Physics and Radar Techniques FHR, 53343 Wachtberg, Germany.

Klaus Aufinger is with Infineon Technologies AG, 85579 Neubiberg, Germany.

Nils Pohl is with the Institute of Integrated Systems, Ruhr University Bochum, 44801 Bochum, Germany, and also with the Fraunhofer Institute for High Frequency Physics and Radar Techniques FHR, 53343 Wachtberg, Germany.

Color versions of one or more figures in this letter are available at https://doi.org/10.1109/LMWT.2024.3389061.

Digital Object Identifier 10.1109/LMWT.2024.3389061

Furthermore, the detection of tiny particles [6], [7] and the classification of materials, either solid [8] or gaseous [9], is enhanced by the use of THz signals. Finally, THz radiation offers significant advantages in medical [10], [11] and security [12], [13] applications. In THz research, silicon technologies are vital, since they enable highly integrated solutions by combining the digital and RF domains, including on-chip antennas, into one chip. Moreover, integrated on-chip antennas can eliminate off-chip transitions and the need for RF PCBs [14] and show improved efficiency when increasing the frequency to THz [15], [16].

This letter introduces a 360-GHz subharmonic mixer (SHM) with an on-chip local oscillator (LO) generation for FMCW radar applications using the 90-nm B12HFC silicon–germanium (SiGe) BiCMOS technology from Infineon [2], [17], featuring an $f_T/f_{\max} = 300/500$ GHz. The circuit design and fabricated MMIC are detailed in Section II. Section III analyzes the mixer's simulation and measurement results, which are compared against other SiGe mixers in Section IV. Finally, Section V concludes this letter.

II. Circuit Design

THz transceiver circuit designs often employ harmonic approaches due to the technology's transit frequency limitations. While SHM circuits may experience reduced conversion efficiency [18], they eliminate the need for additional frequency doubler or PA stages [19]. This trade-off can result in a more compact MMIC footprint and lower power consumption.

Fig. 1 shows the block diagram and the breakout chip, including a transmit (Tx) path and a receive (Rx) path. While the 360-GHz Tx path was presented in [20] and [21], this letter describes the Rx path depicted in the block diagram and focuses on the SHM.

A Colpitts–Clapp VCO on the breakout MMIC generates a 90-GHz LO signal. This signal is subsequently doubled to 180 GHz using a Gilbert-cell-based frequency doubler. The 180-GHz signal is then amplified by a two-stage PA, as described in [20] and [21]. After amplification, the LO signal is split and routed to both the Tx path, described in [21], and Rx path [see Fig. 1(b)]. The Rx path begins with a 90° hybrid coupler, generating in-phase (I) and quadrature-phase (Q) signals (detailed in [21]). These IQ signals are then amplified by the same two-stage PAs and fed into the SHM, whose size is $200 \times 140\ \mu\mathrm{m}^2$. To characterize the SHM,

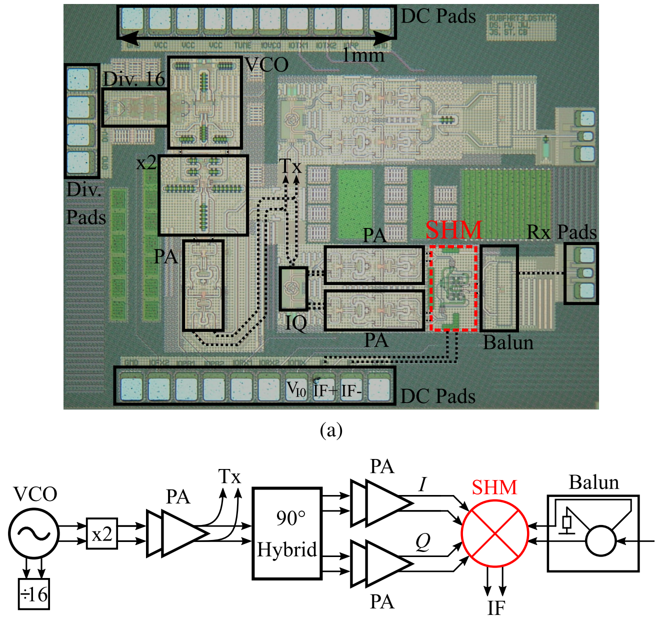

(a)

(b)

Fig. 1. (a) Photograph and (b) block diagram of the 360-GHz subharmonic receiver, including the VCO, frequency divider, frequency doubler, PA stages, the balun, Lange coupler, and the SHM (red dotted box).

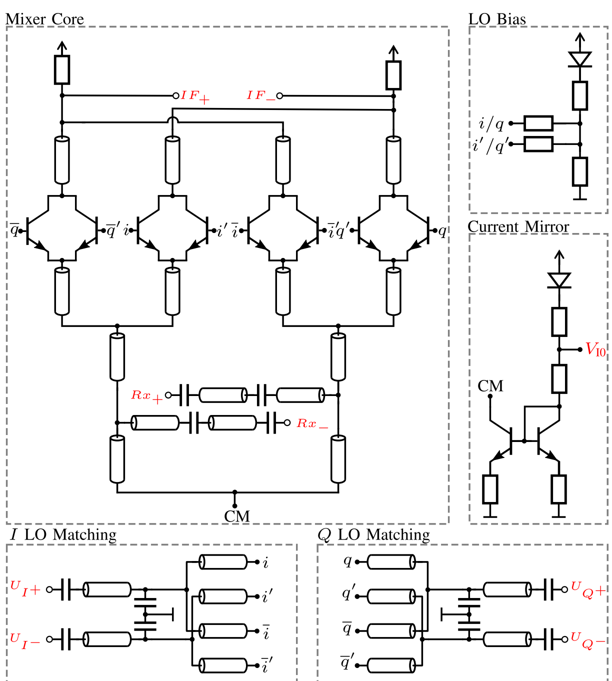

Fig. 2. Circuit diagram of the SHM, including the matching network, the current mirror, and the bias network. External signals are marked in red, and internal signals are marked in black. The current density of the HBTs can be adjusted by applying a voltage to V_{I0}.

a synthetic 360-GHz Rx signal is applied using single-ended RF pads and an on-wafer probe. This signal is then converted to a differential signal using a rat-race balun.

The circuit diagram of the balanced SHM is shown in Fig. 2, highlighting key sections: the mixer core, the LO bias network for the HBT pairs, the current mirror circuitry, and the matching networks for the I and Q inputs. The mixer core utilizes a Gilbert-cell topology with an integrated push–push-

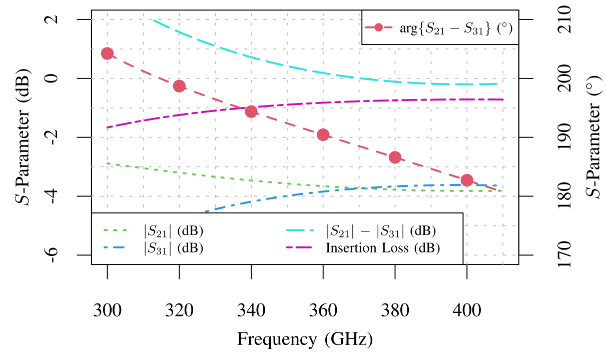

Fig. 3. Simulation results of the rat-race balun showing the amplitude and phase difference, insertion loss, and transmission behavior using sonnet. The circular marker shows the phase difference (right axis).

based frequency doubling mechanism, enabling subharmonic operation.

To maximize conversion gain, several design choices were implemented in conjunction. First, the RF signal is directly coupled to the mixer core, bypassing HBTs (typically used as transconductance stages). Since the HBTs operate above their f_T, they cannot provide current gain. In addition, direct coupling can improve broadband matching [19].

Omitting the transconductance stages increases the available power supply headroom for utilizing large load resistors to enhance conversion gain. However, a limited 3.3-V power supply and large resistors could lead to suboptimal current densities (impacting f_T) and inadequate base–collector voltages (affecting compression behavior). We found that 1200-Ω polysilicon resistors provide a good balance, meeting our design criteria.

Within the mixer core, we utilize compact 1.8-μm BEBC HBTs. These allow operation with low dc currents while maintaining sufficient f_T and facilitating the use of large load resistors for improved conversion gain. Finally, we jointly designed the matching network of the LO and Rx port to maximize the conversion gain, as their matching influences each other.

Inside the layout of the mixer, we had to cross-multiple transmission lines (TRLs) caused by the Gilbert-cell topology itself and by integrating a push–push topology using IQ signals. The LO and Rx matching networks employ the highest copper layer (M7) and the overlying aluminum layer for TRLs. The connections among the eight collector nodes are established beneath the Rx TRLs using M6-based embedded striplines, with M2 and M7 as the ground plane.

III. Simulation and Measurement Results

Fig. 3 depicts the balun's transmission behavior, including amplitude and phase difference and insertion loss. The input matching is not shown but is better than −17 dB for every port. A modified Lange coupler creates IQ signals, utilizing a vertical TRL coupling topology to minimize its physical size. The simulation shows a phase error of 4°–6° and an amplitude imbalance just below 3 dB [21].

The circuit simulation considers RC parasitics for the resistive load, current mirror, and mixer core. Moreover, it accounts for self-heating using 80 °C device temperature and uses EM simulation results for all TRLs, which are not covered by the manufacturer's models. Due to stability issues in the harmonic

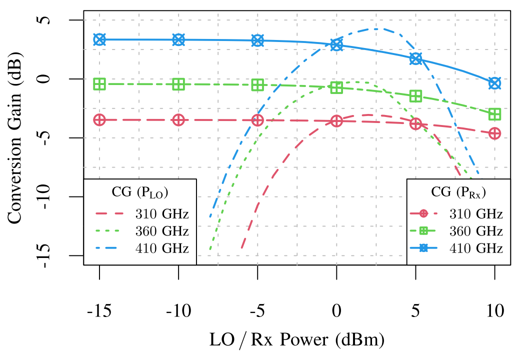

Fig. 4. Simulated CG over LO power (no marker; Rx power = −20 dBm) and simulated CG over RF power (marker; LO power = 0 dBm), including *RC* parasitics, 80 °C device temperature, and ideal IQ and Rx signals.

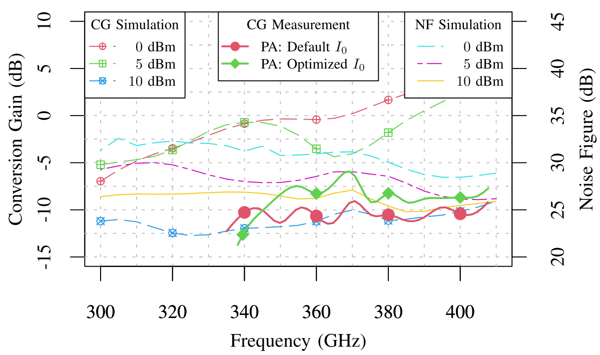

Fig. 5. Simulated NF and conversion gain (*RC* parasitics, 80 °C device temperature, ideal IQ, and Rx signals) and measured conversion gain of the SHM (synthetic Rx signal using a WR2.2 frequency extender and $f_{\mathrm{IF}} \approx 100$ MHz).

balance simulation, we excluded the PAs and couplers and had to use ideal IQ ports.

In Fig. 4, the simulated CG is plotted for varying LO and Rx power levels at a constant IF frequency of 100 MHz. Increasing LO power improves SHM performance until it saturates and then declines from ≈3 dBm onward. Also, excessive Rx power degrades the CG. The 1-dB input compression points were determined at ≈9 dBm (310 GHz), ≈5 dBm (360 GHz), and ≈4 dBm (410 GHz). As frequency rises, compression behavior worsens due to improved Rx matching. Fig. 5 shows the simulated CG and noise figure (NF) for an LO power of 0, 5, and 10 dBm. The simulations show a CG of up to 3.4 dB and a double-sided NF of 24.8 dB when using ideal IQ ports.

We measure the conversion gain using a synthetic receive signal generated by a WR2.2 VNA extender from VDI and a Keysight analog signal generator (E8257D). The IF signal is measured with an oscilloscope (Keysight MSOS804A), which allows for measuring the receiver with its unstabilized VCO in time domain.

As shown in Fig. 4, the SHM has a sweet spot for the optimal LO power of 0–2.5 dBm. But, based on the findings in [20] and [21], we expect an LO power of ≈8 dBm at the SHM's I and Q inputs. Therefore, Fig. 5 depicts the measured conversion gain for two configurations: first, with default (nonoptimized) dc currents (I_0) of the PA's current mirror (similar to Fig. 2), and second, with optimized (slightly decreased) dc currents inside the PA, resulting in up to 6-dB lower LO power. The SHM shows a peak voltage conversion gain of −9.1 dB (default) and −6.1 dB (optimized), with a 3-dB bandwidth of 72 and 57 GHz. Furthermore,

TABLE I
SiGe-Based Mixers Between 300 and 500 GHz

Ref.	$f_{3\,\mathrm{dB}}$ (GHz)	CG (dB)	NF DSB (dB)	P_{DC} (mW)	f_{IF} (MHz)
[22]	343^c	$28^{\clubsuit 1}$	19.7	–	1000
[23]	380^c	$-7.2^{\diamondsuit, \clubsuit 2}$	35	–	–
[24]	480^c	$\approx -14^{\clubsuit 3}$	36.3_{SSB}	33.99	10
[25]	313 – 328	$-14^{\clubsuit 4}$	32_{SSB}	72	100
[26]	325^c	−7.9	30.3	96	33
[27]	300 – 325	$14.8^{\clubsuit 5}$	20	$170^{\sharp}$	50
[28]	480^c	$-8.5^{\clubsuit 4}$	33_{SSB}	13	1000
[29]	474^c	−16	–	–	100
[30]	255 – 310	$-25.75^{\diamondsuit}$	$30^{\diamondsuit}$	58	7000
This	350 – 407	−6.1	$24.8^{\diamondsuit}$	28.4	100

Note: $\clubsuit 1$: including 3-stage IF amplifier, $\clubsuit 2$: including 15 dB single-stage IF amplifier gain, $\clubsuit 3$: including active IF balun, $\clubsuit 4$: including IF buffer, $\clubsuit 5$: including single-stage IF amplifier, $\diamondsuit$: simulated, $\sharp$: including LO buffer, ^{c} : only center frequency available.

we determined the LO to Rx isolation using an H-band spectrum analyzer and probe contacting the Rx pads and measured less than −40 dBm.

IV. Comparison

After characterizing the mixer, we compare it with SiGe-based mixers found in the literature, focusing on those above 300 GHz and below 500 GHz for better comparability. Selected mixers below 300 GHz can be found in [19], [31], [32], [33], [34], [35], [36], [37], [38], [39], [40], [41], [42], and [43], and those above 500 GHz can be found in [18] and [44].

In Table I, we use 3-dB bandwidth, CG, double-sided NF, and power consumption as comparison criteria. Note that conversion gain in some publications includes an IF buffer or an IF amplifier; we deliberately omit this to use SMD amplifiers on the PCB in our upcoming system. Our design demonstrates impressive bandwidth and power consumption characteristics. Notably, it achieves competitive conversion gain despite the absence of an IF buffer or amplifier. We optimized the LO power for peak gain, a capability not available in all compared mixers, contributing significantly to our design's performance. This optimization, the advanced B12HFC SiGe technology, and other design choices contribute to the achieved values of the presented mixer.

V. Conclusion

The presented SiGe-based SHM, designed for THz radar applications, offers a competitive conversion gain of −6.1 dB without additional amplification, an impressive input compression point exceeding 4 dBm, and low-power consumption of 8.6 mA at 3.3 V. These attributes make it well suited for THz radar sensors, which are intended for our future research.

References

[1] D. Kissinger, G. Kahmen, and R. Weigel, "Millimeter-wave and terahertz transceivers in SiGe BiCMOS technologies," *IEEE Trans. Microw. Theory Techn.*, vol. 69, no. 10, pp. 4541–4560, Oct. 2021.

[2] T. Zimmer et al., "SiGe HBTs and BiCMOS technology for present and future millimeter-wave systems," *IEEE J. Microw.*, vol. 1, no. 1, pp. 288–298, Jan. 2021.

[3] P. Hillger et al., "Toward mobile integrated electronic systems at THz frequencies," *J. Infr., Millim., THz Waves*, vol. 41, no. 7, pp. 846–869, Jun. 2020.

[4] J. Wittemeier, F. Vogelsang, D. Starke, H. Rücker, and N. Pohl, "A SiGe based 0.48 THz signal source with 45 GHz tuning range," in *Proc. 51st Eur. Microw. Conf. (EuMC)*, London, U.K., Apr. 2022, pp. 869–872.

[5] D. Starke et al., "A compact and fully integrated FMCW radar transceiver combined with a dielectric lens," *Int. J. Microw. Wireless Technol.*, early access, Dec. 2023. [Online]. Available: https://www.cambridge.org/core/journals/international-journal-of-microwave-and-wireless-technologies/article/compact-and-fully-integrated-text048text thz-fmcw-radar-transceiver-combined-with-a-dielectric-lens/33ED8C6A38F4550E0BD95A775EA532D0#article, doi: 10.1017/S1759078723001368.

[6] T. Bryllert, M. Bonmann, and J. Stake, "A submillimeter-wave FMCW pulse-Doppler radar to characterize the dynamics of particle clouds," *IEEE Trans. Terahertz Sci. Technol.*, vol. 13, no. 4, pp. 389–395, Jul. 2023.

[7] A. Reinhardt, L. Freiwald, T. Jaeschke, N. Pohl, and M. Höft, "A fully integrated SiGe radar sensor for aerosol flow rate measurements," *IEEE Microw. Wireless Compon. Lett.*, vol. 30, no. 2, pp. 216–218, Feb. 2020.

[8] X. Zhang, T. Chang, Z. Wang, and H.-L. Cui, "Three-dimensional terahertz continuous wave imaging radar for nondestructive testing," *IEEE Access*, vol. 8, pp. 144259–144276, 2020.

[9] K. Schmalz, A. Glück, N. Rothbart, A. Güner, M. H. Eissa, and H.-W. Hübers, "Transmitter and receiver in 0.13 μm SiGe for gas spectroscopy at 222–270/444–540 GHz," *IEEE J. Microw.*, vol. 2, no. 4, pp. 582–591, Oct. 2022.

[10] Z. D. Taylor et al., "THz medical imaging: In vivo hydration sensing," *IEEE Trans. Terahertz Sci. Technol.*, vol. 1, no. 1, pp. 201–219, Sep. 2011.

[11] U. R. Pfeiffer et al., "Ex vivo breast tumor identification: Advances toward a silicon-based terahertz near-field imaging sensor," *IEEE Microw. Mag.*, vol. 20, no. 9, pp. 32–46, Sep. 2019.

[12] J. F. Federici et al., "THz imaging and sensing for security applications—Explosives, weapons and drugs," *Semicond. Sci. Technol.*, vol. 20, no. 7, p. S266, Jun. 2005.

[13] K. B. Cooper, R. J. Dengler, N. Llombart, B. Thomas, G. Chattopadhyay, and P. H. Siegel, "THz imaging radar for standoff personnel screening," *IEEE Trans. Terahertz Sci. Technol.*, vol. 1, no. 1, pp. 169–182, Sep. 2011.

[14] S. Thomas, C. Bredendiek, and N. Pohl, "A SiGe-based 240-GHz FMCW radar system for high-resolution measurements," *IEEE Trans. Microw. Theory Techn.*, vol. 67, no. 11, pp. 4599–4609, Nov. 2019.

[15] H. Sobal, "Radiation conductance of open-circuit microstrip (correspondence)," *IEEE Trans. Microw. Theory Techn.*, vol. MTT-19, no. 11, pp. 885–887, Nov. 1971.

[16] B. Sievert, J. T. Svejda, J. Wittemeier, N. Pohl, D. Erni, and A. Rennings, "Equivalent circuit model separating dissipative and radiative losses for the systematic design of efficient microstrip-based on-chip antennas," *IEEE Trans. Microw. Theory Techn.*, vol. 69, no. 2, pp. 1282–1294, Feb. 2021.

[17] P. Chevalier et al., "SiGe BiCMOS current status and future trends in Europe," in *Proc. IEEE BiCMOS Compound Semiconductor Integr. Circuits Technol. Symp. (BCICTS)*, San Diego, CA, USA, Oct. 2018, pp. 64–71.

[18] E. Öjefors, J. Grzyb, Y. Zhao, B. Heinemann, B. Tillack, and U. R. Pfeiffer, "A 820 GHz SiGe chipset for terahertz active imaging applications," in *IEEE Int. Solid-State Circuits Conf. (ISSCC) Dig. Tech. Papers*, San Francisco, CA, USA, Feb. 2011, pp. 224–226.

[19] F. Ahmed, M. Furqan, K. Aufinger, and A. Stelzer, "A SiGe-based wideband 220–310-GHz subharmonic receiver front-end for high resolution radar applications," in *IEEE MTT-S Int. Microw. Symp. Dig.*, Honololu, HI, USA, Jun. 2017, pp. 983–986.

[20] D. Starke et al., "Fully differential 90 GHz and 180 GHz signal sources with tuning ranges of 24.1 GHz and 51.7 GHz in 90 nm SiGe-BiCMOS," in *Proc. 6th Int. Workshop Mobile Terahertz Syst. (IWMTS)*, Bonn, Germany, Jul. 2023, pp. 1–5.

[21] D. Starke et al., "A 360 GHz fully integrated differential signal source with 106.7 GHz continuous tuning range in 90 nm SiGe: C BiCMOS," *IEEE Trans. Microw. Theory Techn.*, early access, 2024. [Online]. Available: https://ieeexplore.ieee.org/abstract/document/10423289, doi: 10.1109/TMTT.2024.3356610.

[22] J. Al-Eryani et al., "Fully integrated single-chip 305–375-GHz transceiver with on-chip antennas in SiGe BiCMOS," *IEEE Trans. Terahertz Sci. Technol.*, vol. 8, no. 3, pp. 329–339, May 2018.

[23] J.-D. Park, S. Kang, and A. M. Niknejad, "A 0.38 THz fully integrated transceiver utilizing a quadrature push-push harmonic circuitry in SiGe BiCMOS," *IEEE J. Solid-State Circuits*, vol. 47, no. 10, pp. 2344–2354, Oct. 2012.

[24] C. Mangiavillano, A. Kaineder, K. Aufinger, and A. Stelzer, "A 1.42-mm^2 0.45–0.49 THz Monostatic FMCW radar transceiver in 90-nm SiGe BiCMOS," *IEEE Trans. Terahertz Sci. Technol.*, vol. 12, no. 6, pp. 592–602, Nov. 2022.

[25] E. Ojefors, B. Heinemann, and U. R. Pfeiffer, "Subharmonic 220- and 320-GHz SiGe HBT receiver front-ends," *IEEE Trans. Microw. Theory Techn.*, vol. 60, no. 5, pp. 1397–1404, May 2012.

[26] K. Statnikov, E. Öjefors, J. Grzyb, P. Chevalier, and U. R. Pfeiffer, "A 0.32 THz FMCW radar system based on low-cost lens-integrated SiGe HBT front-ends," in *Proc. ESSCIRC*, Bucharest, Romania, Sep. 2013, pp. 81–84.

[27] A.-M. Schrotz, S. Breun, V. Issakov, M. Dietz, and R. Weigel, "A 220–325 GHz subharmonic receiver with 14.8 dB peak conversion gain for FMCW radar in SiGe BiCMOS technology," in *Proc. IEEE 22nd Topical Meeting Silicon Monolithic Integr. Circuits RF Syst. (SiRF)*, Las Vegas, NV, USA, Jan. 2022, pp. 74–77.

[28] A. Güner, T. Mausolf, J. Wessel, D. Kissinger, and K. Schmalz, "A 440–540-GHz subharmonic mixer in 130-nm SiGe BiCMOS," *IEEE Microw. Wireless Compon. Lett.*, vol. 30, no. 12, pp. 1161–1164, Dec. 2020.

[29] D. Starke et al., "A fully integrated 0.48 THz FMCW radar transceiver MMIC in a SiGe-technology," in *Proc. 17th Eur. Microw. Integr. Circuits Conf. (EuMIC)*, Milan, IT, Sep. 2022, pp. 56–59.

[30] L. Zhang et al., "Compact multifunctional 180° hybrid based 300 GHz sub-harmonic I/Q down-conversion resistive mixers in 130 nm SiGe process," *IEEE Solid-State Circuits Lett.*, vol. 7, pp. 86–89, 2024.

[31] U. Alakusu et al., "A 210–284-GHz I–Q receiver with on-chip VCO and divider chain," *IEEE Microw. Wireless Compon. Lett.*, vol. 30, no. 1, pp. 50–53, Jan. 2020.

[32] E. Turkmen, I. K. Aksoyak, W. Debski, W. Winkler, and A. Ç. Ulusoy, "A 225–265 GHz IQ receiver in 130-nm SiGe BiCMOS for FMCW radar applications," *IEEE Microw. Wireless Compon. Lett.*, vol. 32, no. 7, pp. 899–902, Jul. 2022.

[33] E. Turkmen et al., "A 223–276-GHz cascadable FMCW transceiver in 130-nm SiGe BiCMOS for scalable MIMO radar arrays," *IEEE Trans. Microw. Theory Techn.*, vol. 71, no. 12, pp. 5393–5412, Dec. 2023.

[34] D. Wang et al., "240-GHz four-channel power-tuning heterodyne sensing readout system with reflection and transmission measurements in a 130-nm SiGe BiCMOS technology," *IEEE Trans. Microw. Theory Techn.*, vol. 67, no. 12, pp. 5296–5306, Dec. 2019.

[35] P. R. Vazquez, J. Grzyb, N. Sarmah, B. Heinemann, and U. R. Pfeiffer, "A 219–266 GHz fully-integrated direct-conversion IQ receiver module in a SiGe HBT technology," in *Proc. 12th Eur. Microw. Integr. Circuits Conf. (EuMIC)*, Nuremberg, Germany, Oct. 2017, pp. 261–264.

[36] N. Sarmah et al., "A fully integrated 240-GHz direct-conversion quadrature transmitter and receiver chipset in SiGe technology," *IEEE Trans. Microw. Theory Techn.*, vol. 64, no. 2, pp. 562–574, Feb. 2016.

[37] Y. Mao, K. Schmalz, J. Borngräber, and J. C. Scheytt, "A 245 GHz CB LNA and SHM mixer in SiGe technology," in *Proc. IEEE 12th Top. Meeting Silicon Monolithic Integr. Circuits RF Syst.*, Santa Clara, CA, USA, Jan. 2012, pp. 5–8.

[38] Y. Mao, K. Schmalz, J. Borngraber, and J. C. Scheytt, "245-GHz LNA, mixer, and subharmonic receiver in SiGe technology," *IEEE Trans. Microw. Theory Techn.*, vol. 60, no. 12, pp. 3823–3833, Dec. 2012.

[39] C. Mangiavillano, A. Kaineder, T. Wagner, and A. Stelzer, "A 240-GHz 4-TX 4-RX 2-D-MIMO FMCW radar transceiver in 130-nm SiGe BiCMOS," *IEEE Microw. Wireless Technol. Lett.*, pp. 1–4, Jun. 2023.

[40] M. H. Eissa et al., "A 220–275 GHz direct-conversion receiver in 130-nm SiGe: C BiCMOS technology," *IEEE Microw. Wireless Compon. Lett.*, vol. 27, no. 7, pp. 675–677, Jul. 2017.

[41] M. Elkhouly et al., "A 240 GHz direct conversion IQ receiver in 0.13 μm SiGe BiCMOS technology," in *Proc. IEEE Radio Freq. Integr. Circuits Symp. (RFIC)*, Seattle, WA, USA, Jun. 2013, pp. 305–308.

[42] D. Fritsche, J. D. Leufker, G. Tretter, C. Carta, and F. Ellinger, "A low-power broadband 200 GHz down-conversion mixer with integrated LO-driver in 0.13 μm SiGe BiCMOS," *IEEE Microw. Wireless Compon. Lett.*, vol. 25, no. 9, pp. 594–596, Sep. 2015.

[43] R. Hasan, M. H. Eissa, W. A. Ahmad, H. J. Ng, and D. Kissinger, "Wideband and efficient 256-GHz Subharmonic- based FMCW radar transceiver in 130-nm SiGe BiCMOS technology," *IEEE Trans. Microw. Theory Techn.*, vol. 71, no. 1, pp. 59–70, Jan. 2023.

[44] E. Öjefors and U. R. Pfeiffer, "A 650 GHz SiGe receiver front-end for terahertz imaging arrays," in *IEEE Int. Solid-State Circuits Conf. (ISSCC) Dig. Tech. Papers*, San Francisco, CA, USA, Feb. 2010, pp. 430–431.